Journal of Alloys and Compounds, 206 (1994) 121–127
JALCOM 1000

Thermodynamic assessment of the Ti–Zr system and calculation of the Nb–Ti–Zr phase diagram

K.C. Hari Kumar, P. Wollants and L. Delaey
Department MTM, Katholieke Universiteit Leuven, de Croylaan 2, B-3001 Heverlee (Belgium)

(Received October 14, 1993)

Abstract

Equilibrium phase relationships in the Nb–Ti–Zr system are computed using the Calphad approach. SGTE-recommended lattice stability expressions for the pure elements are used. The thermodynamic model parameters for Nb–Ti and Nb–Zr are taken from recent assessments. A new thermodynamic description of Ti–Zr is obtained by optimizing available experimental thermochemical and phase diagram data. Phase diagrams of the three limiting binaries, liquidus projection, solidus projection and a number of isothermal sections are computed.

1. Introduction

Knowledge of the thermodynamics and phase diagram of the Nb–Ti–Zr system is of significant technological relevance. Titanium alloys exhibit superior creep properties and good weldability. Zirconium alloys represent an important construction material in nuclear reactors.

The equilibrium diagram of Nb–Ti–Zr has been studied by several investigators [1–8]. The results of these studies are rather conflicting. Moreover, the presently accepted version of the Ti–Zr phase diagram [9] does not comply with isothermal sections presented by these authors, especially in the low temperature range. Hence it is desirable to calculate the Nb–Ti–Zr phase diagram using thermodynamic descriptions of lower order systems.

In the present work thermodynamic model parameters for the Nb–Ti and Nb–Zr systems are taken from recent assessments [10, 11]. The thermodynamic description of Ti–Zr is obtained by the least-squares optimization of experimental thermochemical and phase diagram data from the literature. The ternary phase diagram is calculated by combining the binary descriptions according to the Muggianu extrapolation formula [12]. The liquidus projection, solidus projection and several isothermal sections are thus calculated.

2. Thermodynamic models

All equilibrium phases (liquid, b.c.c. and h.c.p.) are modelled using a single-lattice random solution model. According to this model the integral molar Gibbs energy of phase ϕ ($\phi \equiv$ liquid, b.c.c. or h.c.p.) of the ternary alloy is given by

$$G_m^\phi = \sum_{i=\mathrm{Nb,Ti,Zr}} X_i^\phi {}^\circ G_i^\phi + RT \sum_{i=\mathrm{Nb,Ti,Zr}} X_i^\phi \ln X_i^\phi + {}^{ex}G_m^\phi$$

where ${}^\circ G_i^\phi$ is the Gibbs energy of component i in the structural state ϕ and ${}^{ex}G_m^\phi$ is the excess molar Gibbs energy of the ternary. If we use the Redlich–Kister polynomial [13] to describe the excess Gibbs energies of limiting binaries, then according to the Muggianu extrapolation formula [12] the excess Gibbs energy of the ternary alloy can be written as

$${}^{ex}G_m^\phi = X_{\mathrm{Nb}}^\phi X_{\mathrm{Ti}}^\phi L_{\mathrm{Nb,Ti}}^\phi + X_{\mathrm{Nb}}^\phi X_{\mathrm{Zr}}^\phi L_{\mathrm{Nb,Zr}}^\phi + X_{\mathrm{Ti}}^\phi X_{\mathrm{Zr}}^\phi L_{\mathrm{Ti,Zr}}^\phi$$

where

$$L_{i,j}^\phi = {}^0L_{i,j}^\phi + {}^1L_{i,j}^\phi (X_i^\phi - X_j^\phi) + {}^2L_{i,j}^\phi (X_i^\phi - X_j^\phi)^2 + \ldots$$

Numerical values of the Redlich–Kister model parameters (${}^\nu L_{i,j}^\phi$) are usually determined by a weighted least-squares optimization of the selected experimental thermochemical and phase diagram data of the binary in question.

3. Lattice stabilities

Recent SGTE recommendations of lattice stability data for pure elements [14] are used in this work. These are listed in Table 1.

SSDI 0925-8388(93)01000-T

TABLE 1. Lattice stability expressions for Nb, Ti and Zr [14]

ϕ	${}^{\circ}G^{\phi}_{Nb} - {}^{\circ}G^{b.c.c.}_{Nb}$ (J mol^{-1}), Nb lattice stability – reference state b.c.c.
Liquid	$29781.555 - 10.816417T - 3.06098\times10^{-23}T^{7}$ (298.15 < T < 2750.00 K)
	$30169.902 - 10.964695T - 1.52824\times10^{32}T^{-9}$) (2750.00 < T < 6000.00 K)
H.c.p.	$10000 + 2.4T$ (298.15 < T < 6000.00 K)
ϕ	${}^{\circ}G^{\phi}_{Ti} - {}^{\circ}G^{h.c.p.}_{Ti}$ (J mol^{-1}), Ti lattice stability – reference state h.c.p.
B.c.c.	$6787.856 - 65428/T + 1.098972T - 1.5835T\ \ln(T) + 4.11413\times10^{-3}T^{2} - 3.85519\times10^{-7}T^{3}$ (298.15 < T < 900.00 K)
	$6539.75 - 35472/T + 1.726111T - 1.5881T\ \ln(T) + 3.539455\times10^{-3}T^{2} - 1.87926\times10^{-7}T^{3}$ (900.00 < T < 1155.00 K)
	$5758.548 - 525090/T + 38.389841T - 7.4305T\ \ln(T) + 9.363570\times10^{-3}T^{2} - 1.048055\times10^{-6}T^{3}$ (1155.00 < T < 1941 K)
	$151010.046 - 352999304/T - 821.233343T + 106.3083366T\ \ln(T) - 30.213169\times10^{-3}T^{2} + 1.533611\times10^{-6}T^{3}$ (1941.00 < T < 4000.00 K)
Liquid	$12194.415 - 6.980938T$ (298.15 < T < 1300.00 K)
	$368610.36 - 65556856/T - 2620.999038T + 357.005867T\ \ln(T) - 155.262855\times10^{-3}T^{2} + 12.254402\times10^{-6}T^{3}$ (1300.00 < T < 1941.00 K)
	$104639.72 - 36699805/T - 340.070171T + 40.9282461T\ \ln(T) - 8.204849\times10^{-3}T^{2} + 3.04747\times10^{-7}T^{3}$ (1941.00 < T < 4000.00 K)
ϕ	${}^{\circ}G^{\phi}_{Zr} - {}^{\circ}G^{h.c.p.}_{Zr}$ (J mol^{-1}), Zr lattice stability – reference state h.c.p.
Liquid	$18147.69 - 9.080812T + 1.6275\times10^{-22}T^{7}$ (298.15 < T < 2128.00 K)
	$17804.661 - 8.911574T + 1.342895\times10^{31}T^{-9}$ (2128.00 < T < 4000.00 K)
B.c.c.	$7302.056 - 9738/T - 0.70335T - 1.445606T\ \ln(T) + 4.037826\times10^{-3}T^{2} - 9.7289735\times10^{-6}T^{3} - 7.6142894\times10^{-11}T^{4}$ (298.15 < T < 2128.00 K)
	$-4620.034 + 1.55998T + 1.4103475\times10^{32}T^{-9}$ (2128.00 < T < 4000.00 K)

4. Evaluation of solution parameters and calculation of phase diagrams

4.1. Binary systems

The Nb–Ti system was recently assessed by Hari Kumar *et al.* [10]. Guillermet [11] has assessed the Nb–Zr system. Solution parameters obtained in those works are reproduced in Table 2. Computed phase diagrams of Nb–Ti and Nb–Zr using these data are shown in Figs. 1 and 2 respectively. The Ti–Zr phase diagram was previously calculated by a number of authors [9, 15, 16]. However, SGTE-recommended lattice stability expressions for Ti and Zr are significantly different from those used in these calculations. Since those works, new thermochemical and phase diagram data have become available. Hence a reassessment of the thermodynamic description of Ti–Zr is desirable.

4.2. Ti–Zr system

The phase diagram of Ti–Zr shows complete liquid and solid solubility. It is characterized by two congruent transformations: liquid ↔ b.c.c. and b.c.c. ↔ h.c.p. The system was critically evaluated by Murray [9, 16]. The temperatures of the b.c.c ↔ h.c.p. congruent transformation suggested in these evaluations differ by about 70 K.

There are no experimental data regarding the liquidus. The only reliable experimental solidus data are due to Rudy [17], who used the incipient melting technique. There are a number of studies reported in the literature on the b.c.c./h.c.p. phase boundaries [18–28]. The results

TABLE 2. Solution parameters (${}^{\nu}L^{\phi}_{i,j}$) for Nb–Ti, Nb–Zr and Ti–Zr systems

ϕ	ν	${}^{\nu}L^{\phi}_{Nb,Ti}$ (J mol^{-1})
Liquid	0	+3000
B.c.c.	0	+8900
H.c.p.	0	+13150
ϕ	ν	${}^{\nu}L^{\phi}_{Ti,Zr}$ (J mol^{-1})
Liquid	0	−968
B.c.c.	0	−4346+5.489T
H.c.p.	0	+5133
ϕ	ν	${}^{\nu}L^{\phi}_{Nb,Zr}$ (J mol^{-1})
Liquid	0	+10311
	1	+6709
B.c.c.	0	+15911+3.350T
	1	+3919−1.091T
H.c.p.	0	+24411

of the earlier works [18–24] show considerable scatter. The results of the more recent studies [25–28] are more or less in agreement with one another. Murray [9] points out that the classical techniques used in the earlier studies, such as metallography, pose experimental difficulties, especially near equiatomic compositions, owing to the retention of the original transformation microstructure and thermal hysteresis. The earlier studies report a much lower congruent transformation temperature than the more recent ones. A higher congruent transformation temperature appears to be more consistent with the thermodynamics of the system.

Apart from the phase diagram data, there are also a limited number of thermochemical data available in the literature. Auffredic *et al.* [26] and Blacktop *et al.* [27] measured calorimetrically the heat of the b.c.c. ↔ h.c.p. transformation. The results of these studies agree with each other. Peyzulayev *et al.* [29] used levitation melting to measure the activity of Ti in Zr-rich liquid alloys. Zee *et al.* [30] measured the vapour pressure of Ti over Zr–4 at.% liquid alloy. The results of these studies show that the liquid phase is very nearly ideal.

In the parameter optimization the phase diagram data from refs. 24–28 and the thermochemical data from refs. 26, 27 and 30 were used. Using a weighted least-squares optimization [31] of the selected data, it was possible to obtain a set of model parameters for all stable phases which satisfactorily reproduce the experimental data. The optimized solution parameters obtained in this way are listed in Table 2.

In Table 3 model-calculated values of the b.c.c. ↔ h.c.p. transformation enthalpies are compared with the experimental values. The calculated results are in good agreement with the values reported by Blacktop *et al.* [27]. The calculated phase diagram along

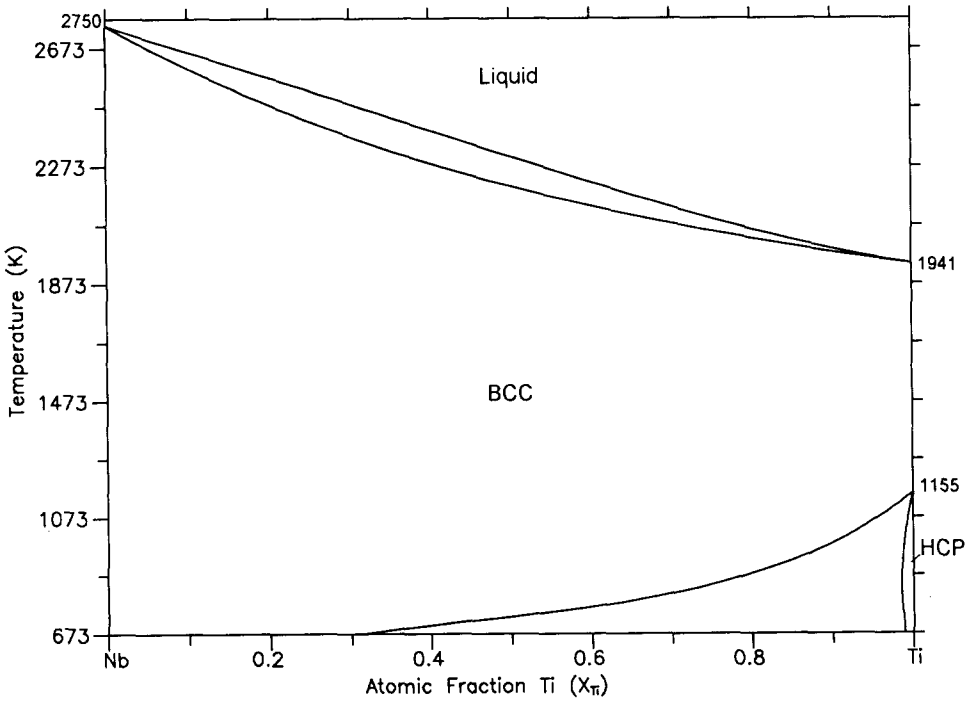

Fig. 1. Computed Nb–Ti phase diagram.

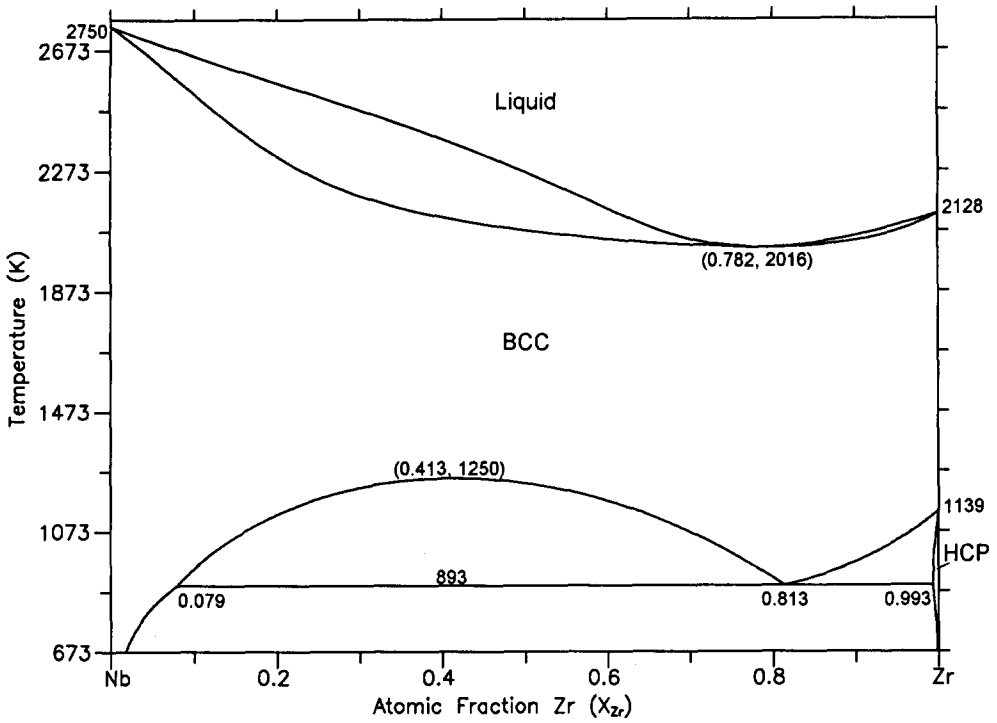

Fig. 2. Computed Nb–Zr phase diagram.

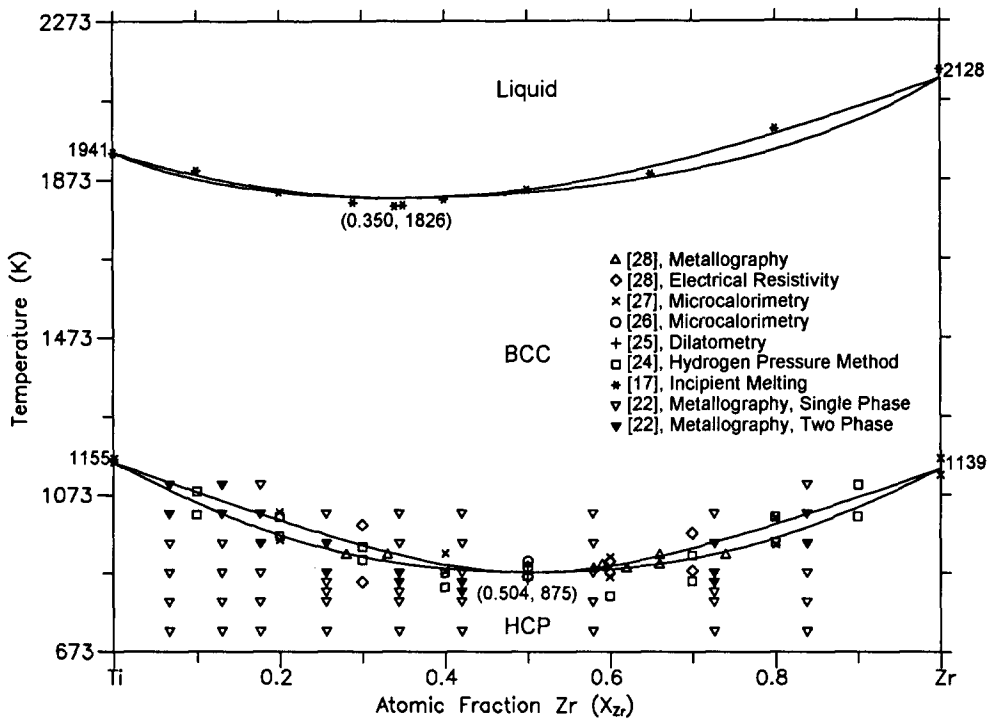

Fig. 3. Computed Ti–Zr phase diagram.

with various experimental data is shown in Fig. 3. The calculated azeotropic minimum of the liquid ↔ b.c.c. congruent transformation is at $X_{Zr}=0.350$, corresponding to 1826 K (1553 °C). Calculations also show that the b.c.c. ↔ h.c.p. congruent transformation occurs at $X_{Zr}=0.504$, corresponding to 875 K (602 °C).

4.3. Ternary system

In a previous work Li Lin [32] has calculated four isothermal sections of the ternary system in the temperature range 620–820 °C. The calculated diagrams show thermodynamic inconsistencies because of the incompatibilities in the thermodynamic descriptions

TABLE 3. Heat of b.c.c.→h.c.p. congruent transformation of Ti–Zr alloys

X_{Zr}	T (K)	Heat of transformation (J mol^{-1})		Reference
		Calculated	Experimental	
0.2	993	−3421	−3376	27
0.4	911	−3050	−3338	27
0.6	903	−3120	−3385	27
0.8	998	−3427	−3730	27
0.5	858	−3202	−2460	26
0.5	888	−3073	−2520	26

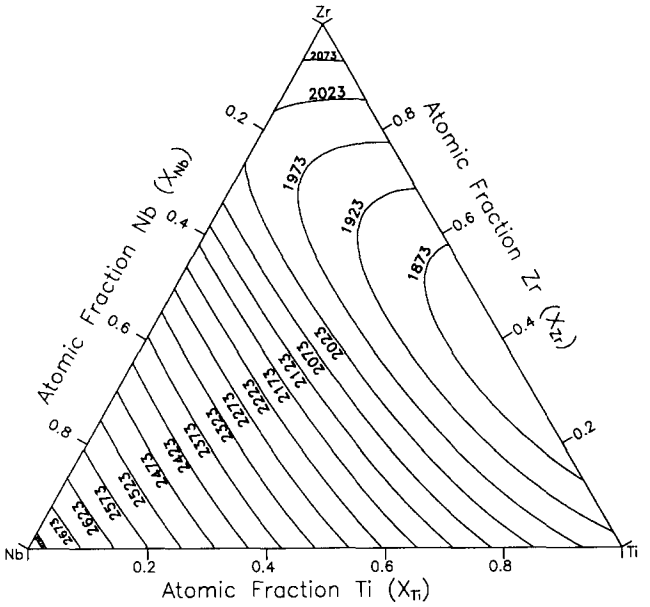

Fig. 4. Nb–Ti–Zr: computed liquidus projection (indicated temperatures are in kelvins).

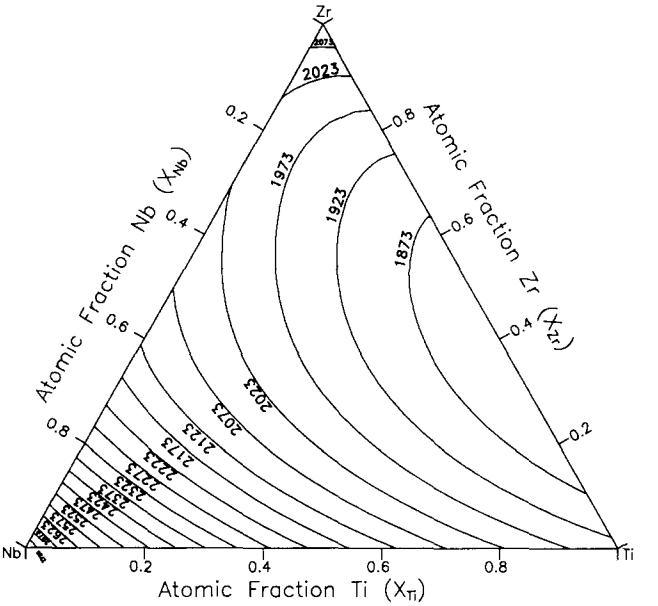

Fig. 5. Nb–Ti–Zr: computed solidus projection (indicated temperatures are in kelvins).

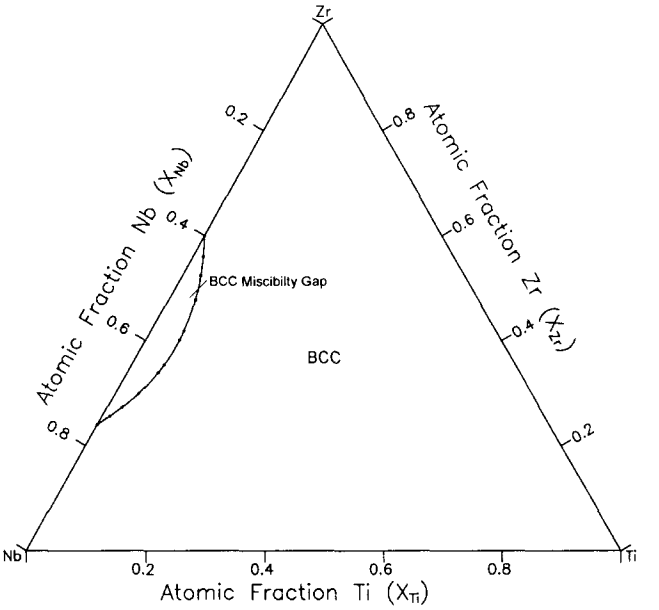

Fig. 6. Nb–Ti–Zr: computed isothermal section at 1173 K (900 °C).

used. In this work the thermodynamic descriptions of the pure elements and the limiting binaries described above are employed to compute the phase relationships in the ternary.

The computed liquidus projection (Fig. 4) and solidus projection (Fig. 5) show similar topologies. There are no ternary invariant reactions present on the surfaces. The liquidus and solidus temperatures increase with increasing Nb content. The liquidus and solidus isotherms between 2750 K (2477 °C) and 2128 K (1855 °C) originate on the Nb–Ti side and terminate on the Nb–Zr side. The azeotropic minimum of the Nb–Zr system introduces two branches in the liquidus and solidus lines between 2128 K (1855 °C) and 2016 K (1743 °C): one branch closing on the Ti–Zr edge and the other on the Nb–Ti edge. Between 2016 K (1743 °C) and 1941 K (1668 °C) the liquidus and solidus isotherms start on the Nb–Ti edge and end on the Ti–Zr edge. The existence of the azeotropic minimum in Ti–Zr causes all liquidus and solidus isotherms between 1941 K (1668 °C) and 1826 K (1553 °C) to start and end on the Ti–Zr side.

Figure 6 is the isothermal section at 1173 K (900 °C). Only the b.c.c. phase is stable at this temperature. The b.c.c. miscibility gap (b.c.c. + b.c.c.') of the Nb–Zr binary is extended to the ternary. The extension of the miscibility gap into the ternary becomes more pronounced as the temperature is lowered. This is evident in the isothermal section at 973 K (700 °C) (Fig. 7). There are also two b.c.c. + h.c.p. two-phase fields at

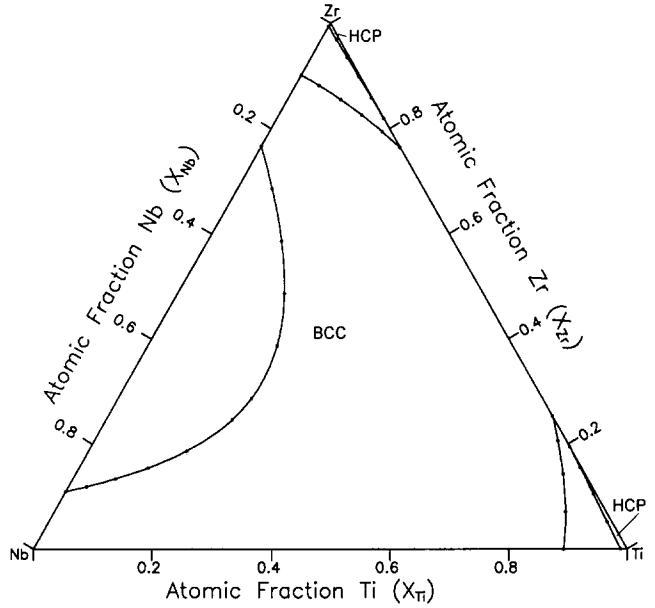

Fig. 7. Nb–Ti–Zr: computed isothermal section at 973 K (700 °C).

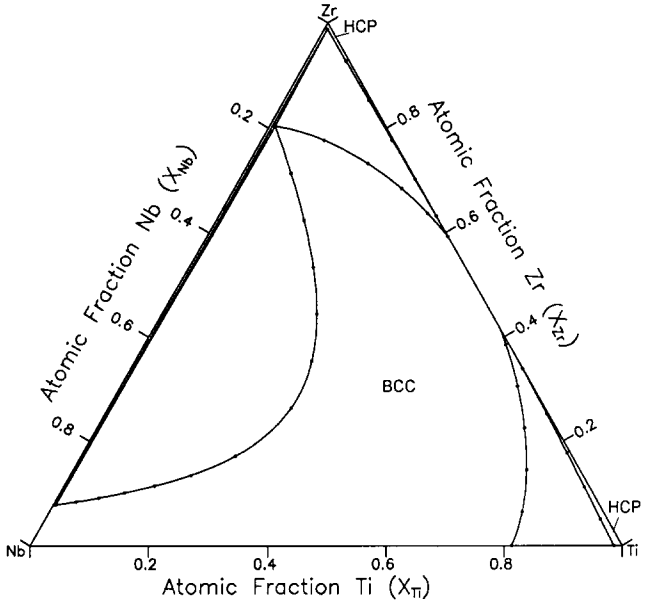

Fig. 8. Nb–Ti–Zr: computed isothermal section at 888 K (615 °C).

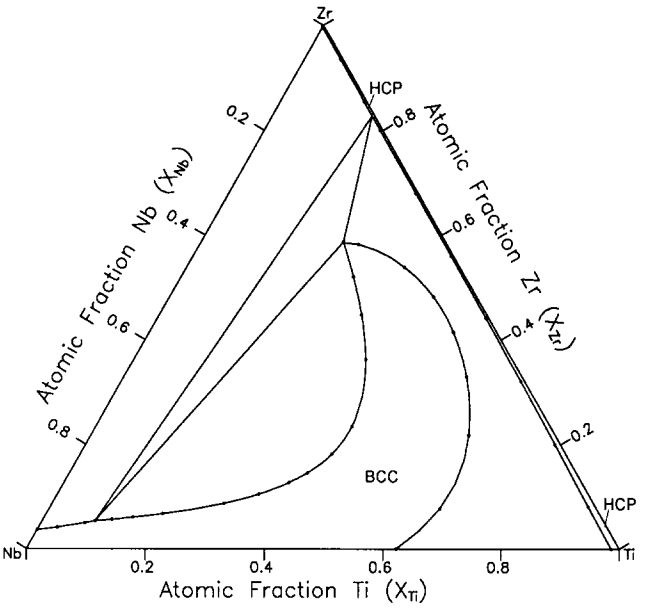

Fig. 9. Nb–Ti–Zr: computed isothermal section at 773 K (500 °C).

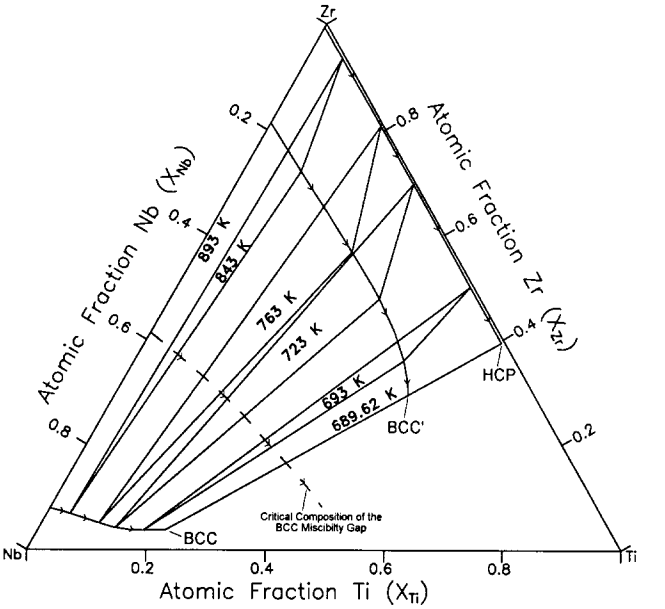

Fig. 10. Nb–Ti–Zr: shift in composition of b.c.c. + b.c.c.′ + h.c.p. tie-triangle.

this temperature, close to the Ti and Zr corners respectively. A thin tie-triangle defined by the three-phase region b.c.c. + b.c.c.′ + h.c.p. close to the Nb–Zr edge is seen in the isothermal section at 888 K (615 °C) (Fig. 8). It is caused by the extension of the monotectoid reaction of the Nb–Zr system (b.c.c. ↔ b.c.c.′ + h.c.p.) into the ternary. Figure 9 is the isothermal section at 773 K (500 °C). At this temperature there exists a narrow region of h.c.p. solid solution along the Ti–Zr side. The tie-triangle is more prominent at this temperature. Figure 10 shows the variation in the composition of the tie-triangle b.c.c. + b.c.c.′ + h.c.p. with temperature. The three-phase region originates as a tie-line at the monotectoid temperature, 893 K (620 °C), of the Nb–Zr system. As the temperature is lowered, it becomes a tie-triangle and finally degenerates to a tie-line inside the ternary at 689.6 K (416.5 °C). The dashed line in Fig. 10 depicts the variation in the composition of the critical point of the b.c.c. miscibility gap with temperature. The isothermal section at 683 K (410 °C) is characterized by a large b.c.c. + h.c.p.

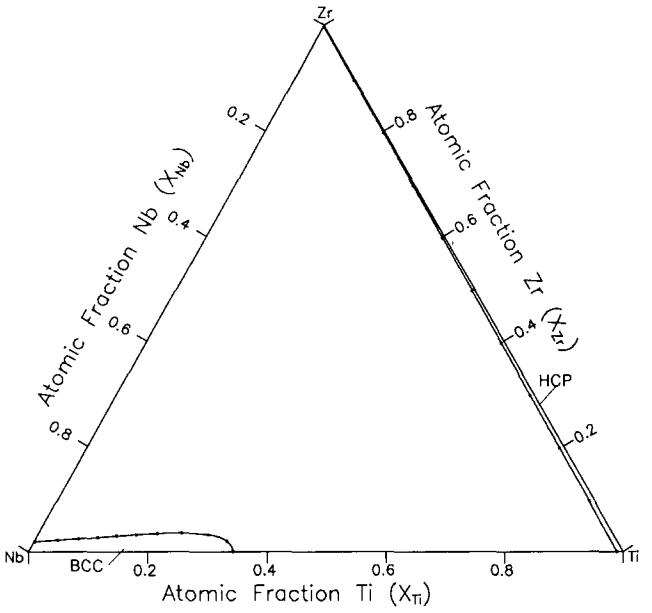

Fig. 11. Nb–Ti–Zr: computed isothermal section at 683 K (410 °C).

field joining the Nb–Ti side and the Nb–Zr side (Fig. 11).

Acknowledgments

The authors wish to thank Dr. H.L. Lukas of the Max-Planck-Institut, Stuttgart, Germany for providing the software (BINGSS) used in the present work. The financial support offered to the Department MTM of the Katholieke Universiteit Leuven by the Flemish Ministry of Education and by the Research Council of Katholieke Universiteit Leuven in the framework of "GOA-Action" is gratefully acknowledged.

References

1 V.S. Mikheev and O.K. Belousov, *Zh. Neorg. Khim., 6* (1961) 1905.
2 T. Doi, H. Ishida and T. Umezawa, *Nippon Kinzoku Gakkaishi, 230* (1966) 139.
3 N.E. Alekseevsky, S.O. Ivanov, I.I. Raevsky and N.V. Stepanov, *Fiz. Met. Metall., 23* (1967) 28.
4 G.N. Kadykova and G.N. Surovaya, *Metall. Obr. Met., 8* (1967) 67.
5 T. Doi, M. Kitada and F. Ishida, *Nippon Kinzoku Gakkaishi, 32* (1968) 684.
6 U. Zwicker, T. Meier and E. Röeschel, *J. Less-Common Met., 14* (1968) 253.
7 P.B. Budberg, U.A. Asonov and I.K. Khegai, *Khim. Redk. Rasseyan. Elem.,* (1969) 126.
8 I.K. Khegay and P.B. Budberg, *Izv. Akad. Nauk SSSR, Met.,* (1) (1971) 206.
9 J.L. Murray, in J.L. Murray (ed.), *Phase Diagrams of Binary Titanium Alloys,* ASM International, Metals Park, OH, 1987, p. 340.
10 K.C. Hari Kumar, P. Wollants and L. Delaey, *Calphad, 18* (1994) 79.
11 A.F. Guillermet, *Z. Metall., 82* (1991) 478.
12 Y.M. Muggianu, M. Gambino and J.P. Bros, *J. Chim. Phys., 72* (1975) 83.
13 O. Redlich and A.T. Kister, *Ind. Eng. Chem., 40* (1948) 345.
14 A.T. Dinsdale, *Calphad, 15* (1991) 317.
15 L. Kaufman and H. Bernstein, *Computer Calculation of Phase Diagrams,* Academic, New York, 1970.
16 J.L. Murray, *Bull. Alloy Phase Diag., 2* (1981) 197.
17 E. Rudy, *Tech. Rep. AFML-TR-65-2,* Part V, 1969 (Wright Patterson Air Force Base).
18 J.D. Fast, *Rec. Trav. Chim., 58* (1939) 973.
19 E.T. Hayes, A.H. Roberson and O.G. Paasche, *U.S. Bur. Mines Rep. Invest. 4826,* 1951.
20 E. Ence and H. Margolin, *Trans. AIME, 221* (1961) 205.
21 A.G. Imgram, D.N. Williams and H.R. Ogden, *J. Less-Common Met., 4* (1962) 217.
22 P.A. Farrar and S. Adler, *Trans. AIME, 236* (1966) 1061.
23 V.V. Kuprina, V.B. Bernard, A.T. Grigor'ev and E.M. Sokolovskaya, *Vest. Mosk. Univ. Khim., 21* (1966) 69.
24 D. Chatterji, M.T. Hepworth and S.J. Hruska, *Metall. Trans., 2* (1971) 1271.
25 E. Etchessahar and D. Debuigne, *Mem. Sci. Rev. Met., 74* (1977) 195.
26 J.P. Auffredic, E. Etchessahar and D. Debuigne, *J. Less-Common Met., 84* (1982) 49.
27 J. Blacktop, J. Crangle and B.B. Argent, *J. Less-Common Met., 109* (1985) 375.
28 M. Ruch and D. Arias, *Scr. Metall. Mater., 29* (1993) 533.
29 Sh.I. Peyzulayev, V.V. Sumin, V.N. Bykov and L.K. Popova, *Izv. Akad. Nauk SSSR, Met.,* (4) (1971) 144.
30 R.H. Zee, J.F. Watters and R.D. Davidson, *Phys. Rev. B, 34* (1986) 6895.
31 H.L. Lukas, E.-Th. Henig and B. Zimmermann, *Calphad, 1* (1977) 225.
32 Li Lin, *Ph.D. Thesis,* Department MTM, Katholieke Universiteit Leuven, 1992.